HEALTH AND MEDICINE

Nanoengineered on-demand drug delivery system improves efficacy of pharmacotherapy for epilepsy

Di Wu[1,2]†, Fan Fei[2]†, Qi Zhang[1], Xia Wang[2], Yiwei Gong[2], Xiaojie Chen[1], Yuyi Zheng[1], Bei Tan[1], Cenglin Xu[1], Hujun Xie[3], Wenjun Fang[4], Zhong Chen[1,2,5]*, Yi Wang[1,2,5]*

Long-term pharmacotherapy, serving as the main therapeutic approach for epilepsy prophylaxis, has suffered from limited efficacy and potential side effects because of the blood-brain barrier (BBB) and untimely medication. Here, we reported a nanoengineered drug delivery system for synergistic brain-targeting delivery and on-demand drug release of antiepileptic drugs (AEDs). The dopamine-pyrrole hybrid system can improve delivery efficiency through a combination of receptor-mediated transcytosis and BBB disruption–enabled transport induced by photothermal conversion of near-infrared light. Incorporation of polydopamine endowed the delivery system with enhanced conductivity and sensitivity, giving sustained (2 hours) and rapid (30 s) drug release in response to epileptiform discharges. Acute, continuous, and spontaneous seizure models validated that the delivery system could inhibit seizures upon epileptiform abnormalities, treated by one-fifth of the conventional dosage. Complemented with satisfactory biosafety results, this "smart" modality is promising to be an effective and safe strategy to improve the therapeutic index of AEDs for epilepsy.

INTRODUCTION

Epilepsy is a chronic brain disorder affecting ~1% of the population worldwide (*1*), characterized by unprovoked and recurrent seizures. Epileptic seizure is caused by abnormal, excessive, and synchronous neuronal activities in the brain (*2*). The epileptic discharges in initial focal areas can quickly spread to the whole brain if prompt actions are not taken to inhibit the electric discharges. Antiepileptic drugs (AEDs) are considered as the mainstay of clinical treatment to control epileptic seizures (*3*). Because of the recurrent feature of epileptic seizure, long-term pharmacotherapy is essential to maintain the plasma concentration of AEDs at a stable range of therapeutic doses. However, conventional AED medication, such as phenytoin (PHT), suffers from narrow therapeutic window and insufficient brain targeting induced by the blood-brain barrier (BBB) (*4*). Moreover, long-term exposure of central nervous system (CNS) to AEDs leads to adverse effects (e.g., impaired cognition, psychiatric problems, and impairment of liver and renal functions) and to drug-resistant epilepsy (*5*). These are exacerbated with the therapeutic regimen for status epilepticus (SE), where patients necessitate regular medication of AEDs to timely control the continuous and repetitive seizures. Failure of SE control results in serious neurological sequelae and a short-term mortality of 15 to 20% (*6*). Thus, it is imperative to improve the therapeutic efficacy and reduce the side effects of AED treatment.

An ideal pharmacotherapy for epilepsy requires (i) on-demand drug release to suppress the epileptic discharges and (ii) efficient penetration of the BBB. In the past decades, to increase the drug concentration in the brain, many efforts have been dedicated to the development of smart drug delivery systems (DDSs) (*7*–*9*). Various nanoparticle-based DDSs for AEDs including polymeric nanoparticle, hydrogel, and protein nanocage with high encapsulation efficiency have shown their advantages over epilepsy control (*10*–*13*). However, the bottleneck still remains, which largely compromises the therapeutic efficacy of current DDS treatment of epilepsy. First, traditional DDS for AEDs could not control the spread of excitatory signals in a timely manner, as the onset of seizures is usually an abrupt and unpredicted event. In the context of long-term medication, the side effects from these DDS treatments are similar with the direct administration, which, at the same time, raises biosafety concerns. Second, there is no effective strategy to maintain the local drug concentration at a high level for a wide therapeutic time window, which is a major concern during continuous seizures. Considering the pathogenetic features of SE, sustained drug release in response to epileptic discharges is envisioned to be a reliable strategy to suppress continuous seizures.

Another challenge of AED medication is the crossing of the BBB, which serves as a protective semimembrane for CNS. To improve BBB crossing, some brain-targeting strategies including receptor-mediated transcytosis and BBB disruption–enabled transport have been developed for BBB penetration (*14*). For example, Angiopep-2 (ANG), a 19-mer peptide, has a strong affinity to the low-density lipoprotein receptor–related protein 1 on the BBB membrane, increasing the BBB crossing efficiency (*15*). Moreover, the BBB can be disrupted with physical stimulus such as hyperthermia (*16*–*18*). Near-infrared light (NIR) irradiation with high spatiotemporal accuracy could create a focal disruption to enhance drug delivery into deep brain tissue in a noninvasive manner (*19*, *20*). Light at the second NIR window (1000 to 1700 nm) with less energy attenuation allows increased penetration depth up to 5 cm (*21*, *22*). Therefore, we hypothesize that a combined strategy of receptor-mediated transcytosis and NIR could synergistically improve AED targeting efficiency to epileptogenic zones. Upon seizure onset, the AEDs could be released in a timely and sustained manner in response to epileptic discharges afterward. However, it begs the following

[1]Key Laboratory of Neuropharmacology and Translational Medicine of Zhejiang Province, School of Pharmaceutical Sciences, Zhejiang Chinese Medical University, Hangzhou 310053, China. [2]Institute of Pharmacology and Toxicology, College of Pharmaceutical Sciences, Zhejiang University, Hangzhou 310058, China. [3]School of Food Science and Biotechnology, Zhejiang Gongshang University, Hangzhou 310018, China. [4]Department of Chemistry, Zhejiang University, Hangzhou 310027, China. [5]Epilepsy Center, Department of Neurology, Second Affiliated Hospital, School of Medicine, Zhejiang University, Hangzhou 310058, China.
*Corresponding author. Email: chenzhong@zju.edu.cn (Z.C.); wang-yi@zju.edu.cn (Y.W.)
†These authors contributed equally to this work.

question: How to integrate these functional motifs in a single available DDS for epilepsy treatment?

Here, we report a multifunctional DDS (PPY-PDA-PHT-ANG) for epilepsy pharmacotherapy via sustained electroresponsive drug release and synergistic brain targeting. The DDS is fabricated by one-pot copolymerization of pyrrole and dopamine, which are monomers of classic conductive conjugated polymer [polypyrrole (PPY)] and biocompatible nature-inspired polymer [polydopamine (PDA)], respectively (Fig. 1A). During the polymerization, the drug molecules PHT were loaded inside the polymeric nanoparticles through noncovalent interactions with PPY and PDA. After cross-linking of two polymers, the as-prepared hybrid nanoparticles showed an improved sensitivity of electric stimuli with a 125-fold increase in conductivity compared to that of pure PPY, rapidly releasing the AEDs in response to epileptic discharges. The enhanced drug loading efficiency and electroresponsive mechanism of the PDA-enabled carrier resulted in sustained AED release under intermittent stimuli, showing potentials for SE suppression. The unique chemistry of PDA enabled successful surface functionalization via Schiff's base reaction, and distinct light absorbance at the second NIR window also endowed the particles with high light-to-heat conversion. These effects synergistically contribute to the effective BBB penetration and efficient AED delivery. Because of the superior features of PDA working as "biological glue" (*23*), all these functional motifs are integrated in one individual DDS. Figure 1B shows a schematic illustration of the epilepsy treatment by synergistic brain targeting and sustained electroresponsive drug release of the nanoparticles. Our study provides a direction for the development of epilepsy "smart" therapy and paves the way for further treatment of other CNS diseases.

RESULTS

Synthesis and characterization of PPY-PDA-PHT-ANG

The drug-loaded polymeric nanoparticles were prepared by taking advantage of the PDA surface chemistry and balancing the chemical forces between each component. First, PHT was used as a model drug encapsulated in the process copolymerization of dopamine and pyrrole at a determined mass ratio. After adding polyvinyl alcohol (PVA) as a stabilizing agent and ammonium persulfate as an oxidant, dopamine and pyrrole monomers could undergo copolymerization and assembly into nanoparticles (fig. S1). Dopamine, pyrrole, and PHT molecules interact with each other through hydrogen bonds, hydrophobic interactions, and π interactions, producing hybrid drug-loaded nanoparticles (PPY-PDA-PHT) (fig. S2). After the synthesis, the drug loading capacity was determined to be 20.4% by calculating the drug concentration in the supernatant. Transmission electron microscopy (TEM) observation revealed a particle size of ca. 80 nm with uniform distribution (Fig. 1C). Smaller nanoparticles could be obtained when using PVA at a higher concentration (fig. S3A), proving the stabilizing effect of PVA polymer chains. The use of other stabilizing agents, such as SDS, Pluronic F127, or cetyltrimethyl ammonium bromide, resulted in irregular polymerization (fig. S3B). Scanning electron microscopy (SEM) observation demonstrated a rougher surface of nanoparticles and higher degree of cross-link with an increase of dopamine concentration, suggesting the coassembly of dopamine and pyrrole (Fig. 1D and fig. S3C). Further ultraviolet-visible-NIR (UV-Vis-NIR) spectrum showed a distinct absorbance of PPY-PDA-PHT hybrid nanoparticles at a NIR range from 750 to 1350 nm (Fig. 1E). The high extinction of the particles holds the potential of photothermal conversion of NIR irradiation. The typical Fourier transform infrared (FTIR) spectrum confirmed the copolymerization of PPY and PDA (fig. S4). The broad band ranging from 3600 to 3300 cm^{-1} can be assigned to the peak of hydroxyl groups of PDA, and the peaks at 1610 cm^{-1} indicated the presence of indole rings in PDA, corresponding to the typical N—H vibrations. Thermogravimetric analysis was conducted from 100° to 800°C (Fig. 1F and fig. S5). The weight curve and the derivative thermogravimetric result of PPY-PDA-PHT showed a sharper decrease than that of PPY-PDA at around 350°C, which is the decomposition temperature of PHT, proving the synthesis of drug-loaded hybrid polymeric nanoparticles. Further nuclear magnetic resonance (NMR) analysis also confirmed the successful incorporation of PHT (fig. S6). Surface modification of the nanoparticles was performed by chemical conjugation with the thiol-PEGylated brain-targeting peptide ANG. The ANG peptide was first linked with thiol-PEG (polyethylene glycol) *N*-hydroxysuccinimide (NHS) ester through esterification (fig. S7). The catechols of PDA on the particle surface then reacted with the thiol groups via Schiff's base reaction under weak basic condition (*24*), giving PEGylated ANG-modified PPY-PDA-PHT nanoparticles (PPY-PDA-PHT-ANG). Zeta potential profiles indicated that the nanoparticles become neutrally charged, proving the surface modification (Fig. 1G). The PEGylated nanoparticles could remain well dispersed in serum-containing medium, while the unfunctionalized samples would severely aggregate in the same medium (Fig. 1H), showing the potential for further in vivo uses. Recent studies revealed that NIR irradiation could be a noninvasive strategy for BBB opening (*17*, *18*). Thus, the NIR photothermal conversion capability of PPY-PDA-PHT-ANG nanoparticles was evaluated with a 1064-nm laser and an infrared thermal camera. Under continuous NIR irradiation, the solution temperature of the polymeric nanoparticles with or without ANG peptide modification quickly increased and plateaued at 65.3° and 67.0°C, respectively, suggestive of efficient photothermal conversion of the nanoparticles (Fig. 1I). The temperature elevation increased with higher power density of irradiation (Fig. 1J). Further studies showed that the nanoparticles exhibited similar photothermal conversion performance in continuous five "heat-cool" cycles (Fig. 1K), proving its good photostability. The photothermal conversion efficiency of the PPY-PDA-PHT-ANG nanoparticles was determined to be 39.4% (fig. S8). The good performance of photothermal conversion of NIR irradiation paves the way for hyperthermia-enabled BBB penetration.

In vitro electroresponsive drug release and BBB penetration

Drug release behavior under electric stimulus is the key factor of therapeutic efficacy for epilepsy control. To simulate drug release during abnormal epileptiform activity, drug-loaded nanoparticles were predeposited on a platinum (Pt) electrode with specific electric stimulus. Drug concentration changes were analyzed by high-performance liquid chromatography (HPLC) with a UV detector (Fig. 2A). The mass ratio of dopamine and pyrrole largely affected the release performance. Drug-loaded nanoparticles with 5% mass ratio of dopamine released the highest amount of drug molecules under 200 μA of electric stimuli for 10 min (Fig. 2B).

To investigate the effects of dopamine on drug release performance, the electrical conductivity of nanoparticles with different mass ratio of dopamine from 0 to 8% was measured by a standard

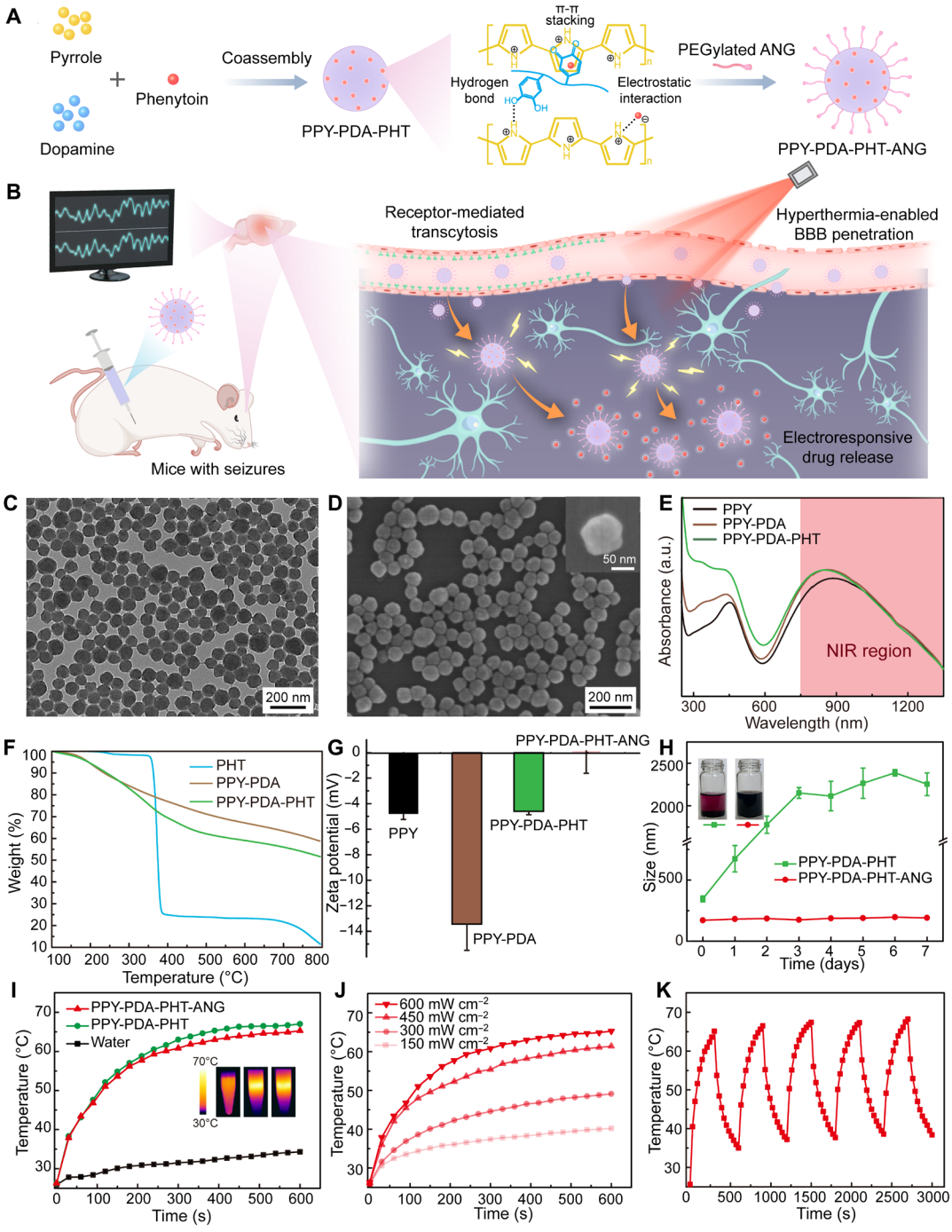

Fig. 1. Characterization of electroresponsive DDS for enhanced epilepsy therapy. (**A**) Schematic illustration of the synthesis of electroresponsive brain-targeting nanoparticles. (**B**) Scheme of epilepsy therapy by intraperitoneal injection of PPY-PDA-PHT-ANG nanoparticles and NIR irradiation using a 1064-nm laser. (**C**) Transmission electron microscopy (TEM) image and (**D**) scanning electron microscopy (SEM) image of the PPY-PDA-PHT nanoparticles. Inset: Magnified SEM image of a single PPY-PDA-PHT nanoparticle. (**E**) Ultraviolet-visible-NIR (UV-Vis-NIR) spectrum of PPY, PPY-PDA, and PPY-PDA-PHT nanoparticles in a wavelength range from UV to the second NIR biowindow. The NIR range was highlighted in red. a.u., arbitrary units. (**F**) Thermogravimetry profiles of PHT, PPY-PDA, and PPY-PDA-PHT from 100° to 800°C with a scanning speed of 10°C per minute. (**G**) Zeta potential results of PPY, PPY-PDA, PPY-PDA-PHT, and PPY-PDA-PHT-ANG nanoparticles in a neutral buffer. (**H**) Dynamic laser scattering analysis of PPY-PDA-PHT nanoparticles with and without surface modification after incubation in serum-containing medium for 7 days ($n = 3$). Inset: Representative photographs of the PPY-PDA-PHT and PPY-PDA-PHT-ANG solutions after 7 days of incubation. (**I**) Temperature increasing profiles of PPY-PDA-PHT and PPY-PDA-PHT-ANG solution (1 mg ml^{-1}) under 1064-nm NIR irradiation at a power density of 600 mW cm^{-2}. Inset: Representative photographs of the solutions acquired by using an infrared thermal camera. (**J**) Temperature increasing profiles of PPY-PDA-PHT-ANG solution (1 mg ml^{-1}) under 1064-nm NIR irradiation at varying power density. (**K**) Photothermal stability of PPY-PDA-PHT-ANG solution in five consecutive photothermal heating (600 mW cm^{-2}) and natural cooling cycles.

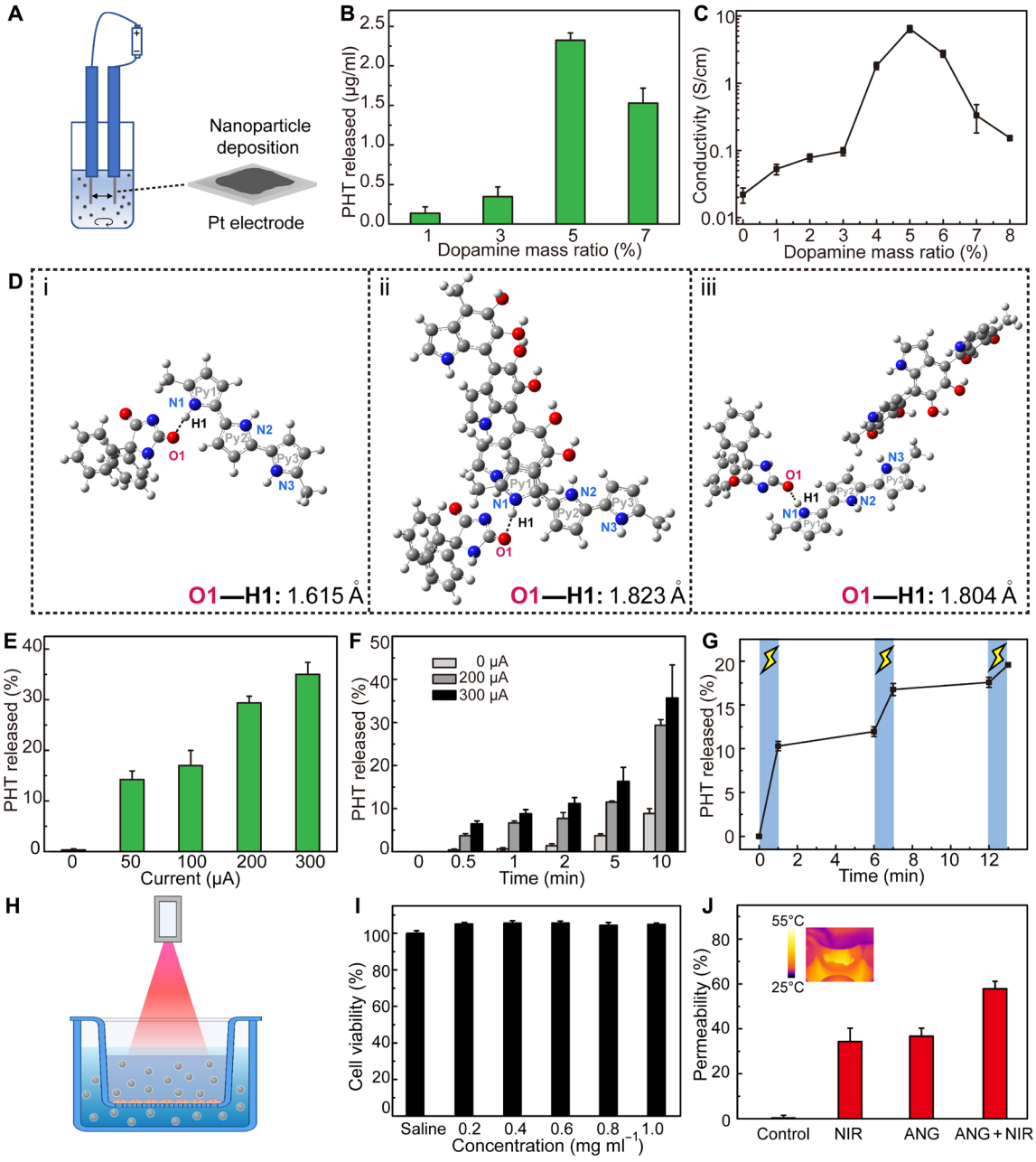

Fig. 2. Electroresponsive behavior and photothermal conversion of the drug-loaded nanoparticles. (**A**) Schematic illustration of a hand-made electric-field device with a pair of Pt electrodes. Nanoparticles were predeposited on the electrode before the study. (**B**) Drug release profiles of the nanoparticles with different dopamine mass ratios under a 200-μA current for 10 min ($n = 3$). (**C**) Plots of electrical conductivity versus dopamine mass ratio measured by a four-point probe setup ($n = 3$). (**D**) Optimized geometry of PHT molecule and PPY polymer chain (i) in the absence and (ii and iii) in the presence of PDA molecule. Geometry (ii) and (iii) represents the PDA molecule interacting with the second and the third PPY molecule, respectively. (**E**) Drug release profiles of the nanoparticles versus current intensity after electric stimulus for 10 min ($n = 3$). (**F**) Drug release profiles of the nanoparticles versus stimulation time after electric stimulus at different current intensities ($n = 3$). (**G**) Sustained drug release profiles of the nanoparticles after "on-off" cycles of electric stimulus. The "on" state represents electric stimulus with a current of 200 μA for 1 min ($n = 3$). (**H**) Schematic illustration of an in vitro BBB model with NIR irradiation. (**I**) Cell viability of the cells treated by drug-loaded nanoparticles up to 1 mg ml^{-1} ($n = 5$). (**J**) In vitro BBB-penetrating ability evaluation during various treatments. Control: PHT; NIR: PPY-PDA-PHT with NIR irradiation (300 mW cm^{-2}); ANG: PPY-PDA-PHT-ANG; NIR + ANG: PPY-PDA-PHT with NIR irradiation (300 mW cm^{-2}). Inset: Representative photograph of the cell culture chamber ($n = 5$).

four-point probe setup. The results indicated that incorporation of dopamine substantially improved the conductivity of nanomaterials, which peaked at 5% of mass ratio, giving a 125-fold increase compared to that of pure PPY (Fig. 2C). Experiments in wet condition also confirmed that the hybrid nanoparticles with a dopamine ratio of 5% have the highest conductivity (fig. S9). To reveal the possible mechanism of this improvement, the molecular model of PPY with three pyrrole molecules in a row and a PHT drug molecule bonding with the first pyrrole ring (Py1) was established (Fig. 2D). The PPY-PDA-PHT-ANG models with three 5, 6-indolequinone molecules

in a row bonding with either the second pyrrole molecule (Py2) or the third pyrrole molecule (Py3) were structured to study the influence of PDA. The density functional theory [M06 functional 6-31G(d)] calculations demonstrated that the incorporation of dopamine elongated the O—H bond length between PPY and PHT, irrespective of the position. Compared with the PPY-PHT model, the intermolecular interactions of O—H bonds in the Py2 and Py3 models decreased from 74.8 kcal mol^{-1} to 63.7 kcal mol^{-1} and to 66.2 kcal mol^{-1}, respectively. Considering the three-dimensional structure of polymeric PPY-PDA-PHT-ANG nanoparticles, it is reasonable to infer the magnified improvement of electroresponsive performance. In addition, the negatively charged PDA molecules introduced free electrons in PPY main chains, increasing the conductivity (*25*). Upon electric stimulus, the PPY chains were reduced and then repulsed the negatively charged PHT molecules, with PDA incorporation facilitating the process. However, excessive addition of dopamine (>5%) would decrease the electrical conductivity (Fig. 2C), as the incorporation of catechol derivatives may shorten the linear PPY structure and limit the charge hopping to lower overall conductivity (*26*). Therefore, further drug release studies were conducted by using PPY-PDA-PHT-ANG nanoparticles with a dopamine mass ratio of 5%.

The current from 50 to 300 μA (5 to 30 mV mm^{-2}), which is similar to the extracellular field potential, was applied in the present study to evaluate the drug release performance (*27*). The results indicated that an electric field of 50 μA is capable of triggering drug release (Fig. 2E). Moreover, nearly 10% of drugs could be released under the electric stimulus for 30 to 60 s (Fig. 2F), suggesting the potential of rapid drug release upon seizure onset. In contrast to the electroresponsive hydrogel in our previous report, PPY-PDA-PHT-ANG released limited drugs under no electric stimulus after 24 hours of incubation (fig. S10), indicating a different release mechanism from that of swelling hydrogels (*10*). Of greater importance, the PPY-PDA-PHT nanoparticles enabled a sustained drug release in response to the intermittent discharges. While treated with an "on-off" cycle of electric stimulus, the drugs were released accordingly at "on" state and showed negligible leaking at "off" state (Fig. 2G). Note that the limited drug release was observed with other stimulus such as NIR irradiation or electromagnetic field, proving the good stability of the nanosystem (fig. S11). This excellent performance of drug release paves a way to control repeated seizures in epilepsy.

Encouraged by the superior photothermal effect, an in vitro BBB model by the bEnd.3 cellular monolayer was established to assess whether drug-loaded nanoparticles could penetrate the BBB (Fig. 2H). The cell viability results confirmed that the nanoparticles up to 1 mg ml^{-1} have no cytotoxicity toward the bEnd.3 cells (Fig. 2I). The integrity of the cellular monolayer was monitored by transendothelial electrical resistance (TEER) (*28*). After 7 days of incubation, the TEER value peaked at 200 ohm·cm^{-2}, which meets the requirement of the evaluation (*29*). Less than 1% of the drugs were measured in the nontargeting nanoparticle group, also demonstrating the membrane integrity of the BBB (Fig. 2J). In contrast, 36.8 ± 3.5% and 34.3 ± 5.9% of the drugs were detected in the down chamber after treatment with ANG-modified nanoparticles or nonmodified nanoparticles together with NIR irradiation. The combination of both methods further improved the penetration efficiency (57.8 ± 3.3%), implying a synergistic effect of receptor-mediated transcytosis and BBB disruption–enabled transport. To investigate the impact of NIR irradiation on the BBB, the TEER value of the cellular monolayer was recorded after the irradiation. As shown in fig. S12A, longer irradiation caused lower TEER. However, the cells under the NIR irradiation without PPY-PDA-PHT-ANG incubation showed no TEER changes. It indicated that PPY-PDA-PHT-ANG could convert NIR energy into local hyperthermia to increase the BBB permeability. The NIR-triggered TEER change could quickly return to normal within 10 min after removing the irradiation (fig. S12B). These results supported the idea that NIR could be used for BBB opening by modulating monolayer permeability in a reversible manner.

In vivo antiseizure effect in epilepsy models

For the antiepileptic effect assessment, one of the most frequently used models, the pentylenetetrazole (PTZ) model, was first established to induce acute seizures in rodent (Fig. 3A). Before the induction, the mice were intraperitoneally injected with PPY-PDA-PHT-ANG at a PHT dose of 5 or 10 mg kg^{-1}. Then, the mice head was irradiated with the 1064-nm laser, focusing on the temporal lobe area under the control of a thermal infrared camera. After PTZ induction, the behavior study was conducted according to the Racine scale (*30*), and electrography was also recorded in the following 30 min. Previous reports suggest an elevated surface temperature of the head skin, yet temperature below 43°C with NIR irradiation improves BBB permeability (*17*, *18*). Thus, the optimal power density of irradiation was determined to be 500 mW cm^{-2} (fig. S13). To further verify brain targeting in vivo, the nanoparticles were labeled with fluorescence dye Cyanine5.5 (Cy5.5). After NIR treatment, strong fluorescent signals were observed in the mouse brains (Fig. 3B), particularly in temporal lobe, indicating successful BBB penetration. Signal intensity in the group of synergistic brain targeting (NIR + ANG) was up to about fourfold (405%) than that in the group of nontargeting nanoparticles (Fig. 3C), which is in accordance with the in vitro results. Behavior observations revealed that the administration of ANG-modified drug-loaded (10 mg kg^{-1}) nanoparticles with NIR treatment (PPY-PDA-PHT-ANG-10 + NIR) lowered the seizure stage from 5.2 ± 0.3 to 3.8 ± 0.2 compared with the PHT-only group at the same dose (Fig. 3D). The behavior study confirmed that treatment with PPY-PDA-PHT-ANG-5 + NIR down to 5 mg kg^{-1} was effective in seizure inhibition [$^{**}P < 0.01$, $^{***}P < 0.001$, and $^{****}P < 0.0001$ compared with the control group; $^{\#\#}P < 0.01$ compared with the PHT group at the same dose via one-way analysis of variance (ANOVA) with Dunnett's multiple comparisons test]. Furthermore, the latency results showed that the treatment of PPY-PDA-PHT-ANG-10 + NIR increased the latency to generalized tonic-colonic seizure (GS; stage 6) from 199 to 1800 s, whereas the PHT-10 group has an average latency of 813 s ($^{**}P < 0.01$, $^{***}P < 0.001$, and $^{****}P < 0.0001$ compared with the control group; $^{\#\#}P < 0.01$ compared with the PHT group at the same dose via one-way ANOVA with Dunnett's multiple comparisons test; Fig. 3E). PTZ-induced epilepsy has a high rate of death if the seizure was not inhibited timely. Because of the responsive drug release, the survival rate of epileptic mice was improved after the treatment ($^{**}P < 0.01$ compared between the group of iii-5, iii-10, and saline via chi-square test; Fig. 3F). These results indicated that the acute seizures can be controlled by administration of one-fifth of the conventional dosage (*31*). Moreover, the electroencephalogram (EEG) patterns of epileptic mice indicated that PPY-PDA-PHT-ANG + NIR treatment could reduce the severity of the EEG onset at a dose of 10 mg kg^{-1} (Fig. 3G). Note that the latencies to early stage [stage 2 (S2)] showed no significant differences between each group (fig. S14), suggesting that the

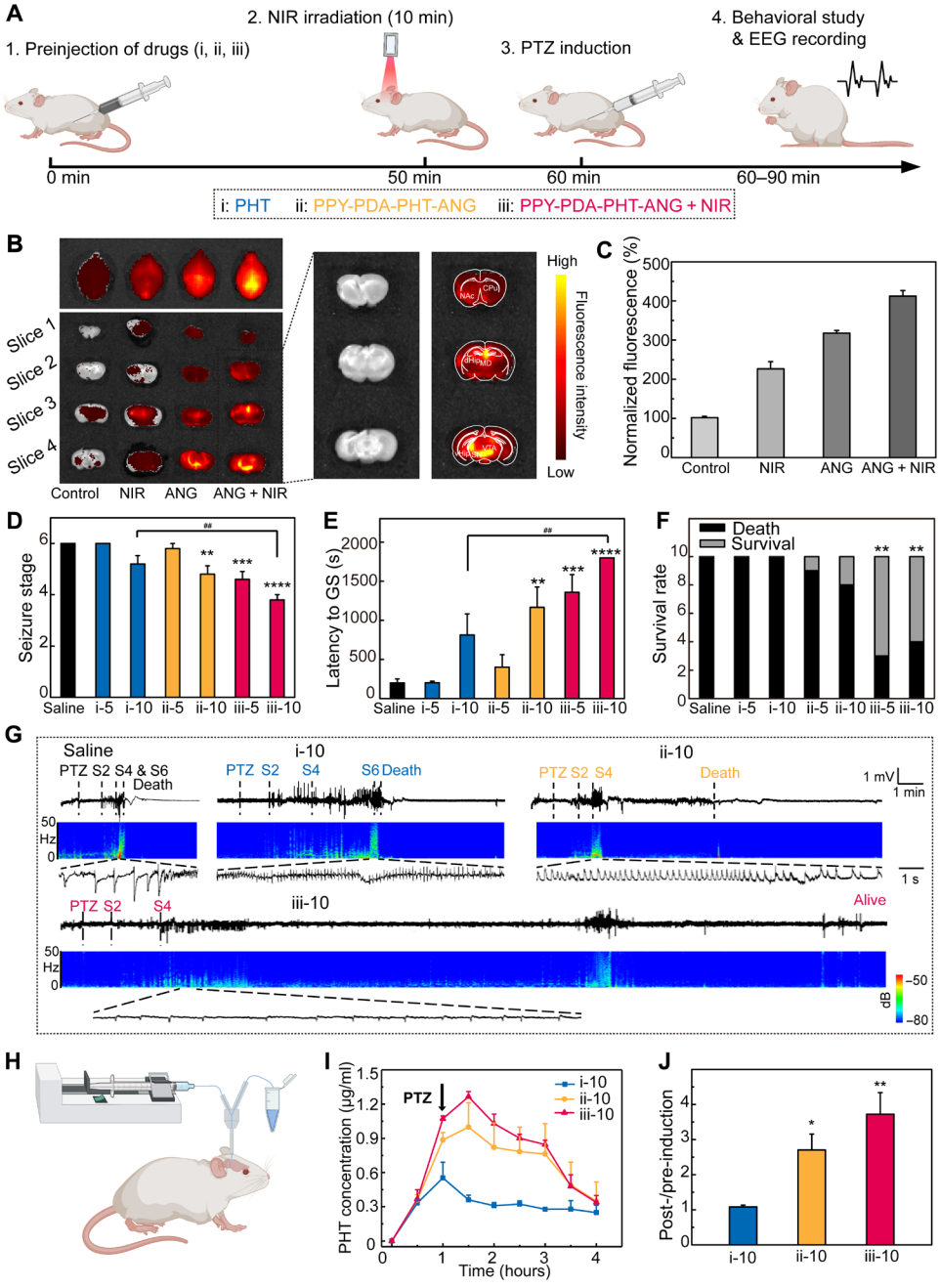

Fig. 3. In vivo antiseizure effects of drug-loaded nanoparticles in PTZ-induced tonic-clonic seizure model. (**A**) Schematic illustration of epilepsy therapy via PPY-PDA-PHT-ANG + NIR. (**B**) Left: Representative fluorescent photographs of brains and brain slices of mice after different treatments. Right: Overlaid image of magnified fluorescent image and Allen Brain Atlas. Both PPY-PDA-PHT and PPY-PDA-PHT-ANG nanoparticles were labeled with Cy5.5 before the study. (**C**) Normalized fluorescence intensity of the brain samples of mice after different treatments ($n = 3$). (**D**) Seizure stage of epileptic mice, (**E**) latency to GS, and (**F**) survival rate in the PTZ-induced seizure model after different treatments of (i) PHT, (ii) PPY-PDA-PHT-ANG, and (iii) PPY-PDA-PHT-ANG + NIR at a dose of 5 or 10 mg kg^{-1} ($n = 10$). (**G**) Representative EEGs and corresponding power spectral analysis recorded from the primary motor cortex of epileptic mice after different treatments at a PHT dose of 10 mg kg^{-1}. (**H**) Schematic illustration of the microdialysis study. The samples were collected and analyzed by HPLC. (**I**) Real-time microdialysis of PHT concentration in brain dialysate of epileptic mice after different treatments at a PHT dose of 10 mg kg^{-1} ($n = 3$). (**J**) Free PHT concentration increase (post/pre) in brain dialysate before and 30 min after seizure induction.

initial epileptic discharges at the lower stage were required to trigger the pharmacotherapy to alleviate seizure spread in later stages.

Thus, to reveal whether the enhanced antiepileptic performance resulted from improved brain targeting and electroresponsive drug release, the real-time PHT drug concentration was recorded by microdialysis of cerebrospinal fluid (Fig. 3H). After 60 min of administration, the drug concentration in the PPY-PDA-PHT-ANG-10 + NIR group was 1.07 μg ml^{-1}, nearly twofold higher that of the PHT-10 group, indicating the enhanced drug accumulation

via synergistic brain-targeting delivery (Fig. 3I). Of greater importance, the concentration in the PPY-PDA-PHT-ANG-10 and PPY-PDA-PHT-ANG-10 + NIR groups was even higher once acute seizure was induced. Specifically, in the PPY-PDA-PHT-ANG-10 + NIR group, the drug concentration 30 min after PTZ-induced epilepsy was 3.7-fold higher than that before the induction (*$P < 0.05$ and **$P < 0.01$ compared with the PHT group at the same dose via one-way ANOVA with Dunnett's multiple comparisons test; Fig. 3J). In the following 2 hours, the drug concentration in the PPY-PDA-PHT-ANG-10 + NIR group fluctuated at a relatively high level because of the sustained drug release. In comparison, the drug concentration in the PHT-10 group decreased after its peak at 60 min because of natural pharmaceutical metabolism. Therefore, the microdialysis results evidenced that the synergistic brain-targeting strategy facilitated drug delivery to the brain, and the drugs could be released in response to epileptic seizures.

Sustained drug release in the brain is key to lower the mortality rate in SE patients. Therefore, we established a pilocarpine-induced epilepsy model, a classic model of clinical SE, to evaluate the therapeutic performance of PPY-PDA-PHT-ANG nanoparticles (Fig. 4A). After drug administration and NIR irradiation, the key indicators including latencies to GS and to SE and the survival rate of SE mice were distinctively improved (****$P < 0.0001$ compared with the control group; $^{\#\#\#\#}P < 0.0001$ compared with the PHT group at the same dose via one-way ANOVA with Dunnett's multiple comparisons test; Fig. 4, B and C, and fig. S15). Energy spectra, representative epileptic EEGs, and the analysis of absolute power during SE are shown in Fig. 4 (D to F) (****$P < 0.0001$ compared with the control group via two-way ANOVA with Tukey's multiple comparisons test). The PPY-PDA-PHT-ANG-10 + NIR treatment distinctively alleviated SE severity at a dose of 10 mg kg^{-1}, whereas PHT administration at the same dose showed almost no therapeutic effects. The energy spectra indicated that the mice with PHT-10 treatment suffered from SE 26 ± 8 min after induction (Fig. 4D). In contrast, the PPY-PDA-PHT-ANG-10 + NIR treatment lowered the incidence of GS (Fig. 4G), and no SE behavior was observed, proving SE inhibition (**$P < 0.01$ compared with the saline group; $^{\#\#}P < 0.01$ compared between the PHT-10 group and the PPY-PDA-PHT-ANG-10 + NIR group via chi-square test). This superior performance convincingly proved that PPY-PDA-PHT-ANG nanoparticles were capable of sustained drug release, which is in accordance with the drug release profiles in Fig. 2G.

To give a comprehensive study of the therapeutic effect, kainic acid (KA)–induced chronic epilepsy model was established as a recurrent and spontaneous seizure model. Three to 5 weeks after the KA induction, the mice turned into a period of spontaneous and recurrent seizure (Fig. 4H). Until the main indicators became stable, the therapeutic treatment was conducted. As shown in Fig. 4 (I and J), after PPY-PDA-PHT-10 + NIR treatment, the spontaneous seizures were inhibited as the GS number and duration were both decreased (*$P < 0.05$ and **$P < 0.01$ compared with the saline group via one-way ANOVA with Dunn's multiple comparisons test). Further EEG study indicated that PPY-PDA-PHT-10 + NIR treatment could reduce the severity of GS at a dose of 10 mg kg^{-1} (Fig. 4K). However, administration of PHT alone showed no effects at the same dose. The GS number and duration in the PHT group have no difference among the days of pretreatment, treatment, and posttreatment (Fig. 4, L and M). Note that, in the KA-induced chronic model, both PHT-10 and PPY-PDA-PHT-10 + NIR have limited effects on the number and duration of nonconvulsive focal seizure (FS) (only effective in a few cases after the treatment of PPY-PDA-PHT-10 + NIR) (fig. S16). This is in accordance with the clinical fact that PHT is mainly effective for GS inhibition. These results together proved that PPY-PDA-PHT-ANG nanoparticles were able to inhibit the spontaneous seizure at a lower AED dose.

In vivo biosafety study

Considering the long-term medication for epilepsy therapy, it is necessary to study the biosafety of the treatment. First, the effect of the treatment on neuromuscular coordination was evaluated via a rotarod test 24 hours after drug administration. The results indicated that there is no difference between the control group and the PPY-PDA-PHT-ANG-10 + NIR group (Fig. 5A). The open-field test, a qualitative and quantitative measurement of exploratory and locomotor activity of rodents, was conducted. The running distance and the mean speed of the four groups showed no significance (Fig. 5, B and C). No activity level change was observed after the treatment of PPY-PDA-PHT-ANG-10 + NIR (Fig. 5D). The fluorescent staining of neurons in the brain was performed to study the neurotoxicity of the treatment, as shown in Fig. 5E. No cell loss was recorded in the view of the coronal plane of the brain, as well as the magnified staining images in hippocampus regions. To further prove long-term biosafety, mice were treated with PPY-PDA-PHT-ANG-10 + NIR once a day for 1 week. The fluorescence images of neurons, astrocytes, and microglia in epileptic regions including the hippocampal CA1, CA3, and cortex were shown in figs. S17 to S19. These fluorescent results indicated that PPY-PDA-PHT-ANG-10 + NIR treatment did not cause any damage to the normal brain, suggesting long-term biosafety. Blood chemistry analysis also showed no significant difference in hematological parameters including total protein, albumin, globulin, total bilirubin, alanine aminotransferase (ALT), aspartate aminotransferase (AST), and blood urea nitrogen (BUN) between each group, confirming the negligible impact on hepatic and renal functions (Fig. 5F). Immunohistological staining of major organs, including the heart, liver, spleen, lung, and kidney, was performed (fig. S20). Compared with the saline group, the results for the groups treated with PPY-PDA-PHT-ANG-10 + NIR exhibited imperceptible organ damages. These studies collectively confirmed the biosafety and biocompatibility of our delivery strategy for epilepsy treatment.

DISCUSSION

Despite the development of AEDs for epilepsy therapy, long-term medication of AEDs could cause many side effects and lead to drug-resistant epilepsy, aggravating brain damages (*32*). The persistence of epilepsy with unprovoked seizures requires higher drug delivery efficiency and precise and sustained drug release in the brain to inhibit the epileptic discharge in time. Previous studies mainly focused on the development to improve the delivery efficiency of AEDs. Notably, some nanoscaled DDSs have been developed to deliver more AEDs into brains (*33*, *34*). However, the DDSs with on-demand drug release for stimuli-responsive epilepsy treatment have rarely been investigated. On the basis of the pathological characteristics of abnormal and excessive discharges upon seizure onset, an electroresponsive delivery system could be a potential avenue for effective epilepsy treatment. We have previously reported an electroresponsive hydrogel system for epilepsy control (*10*). However,

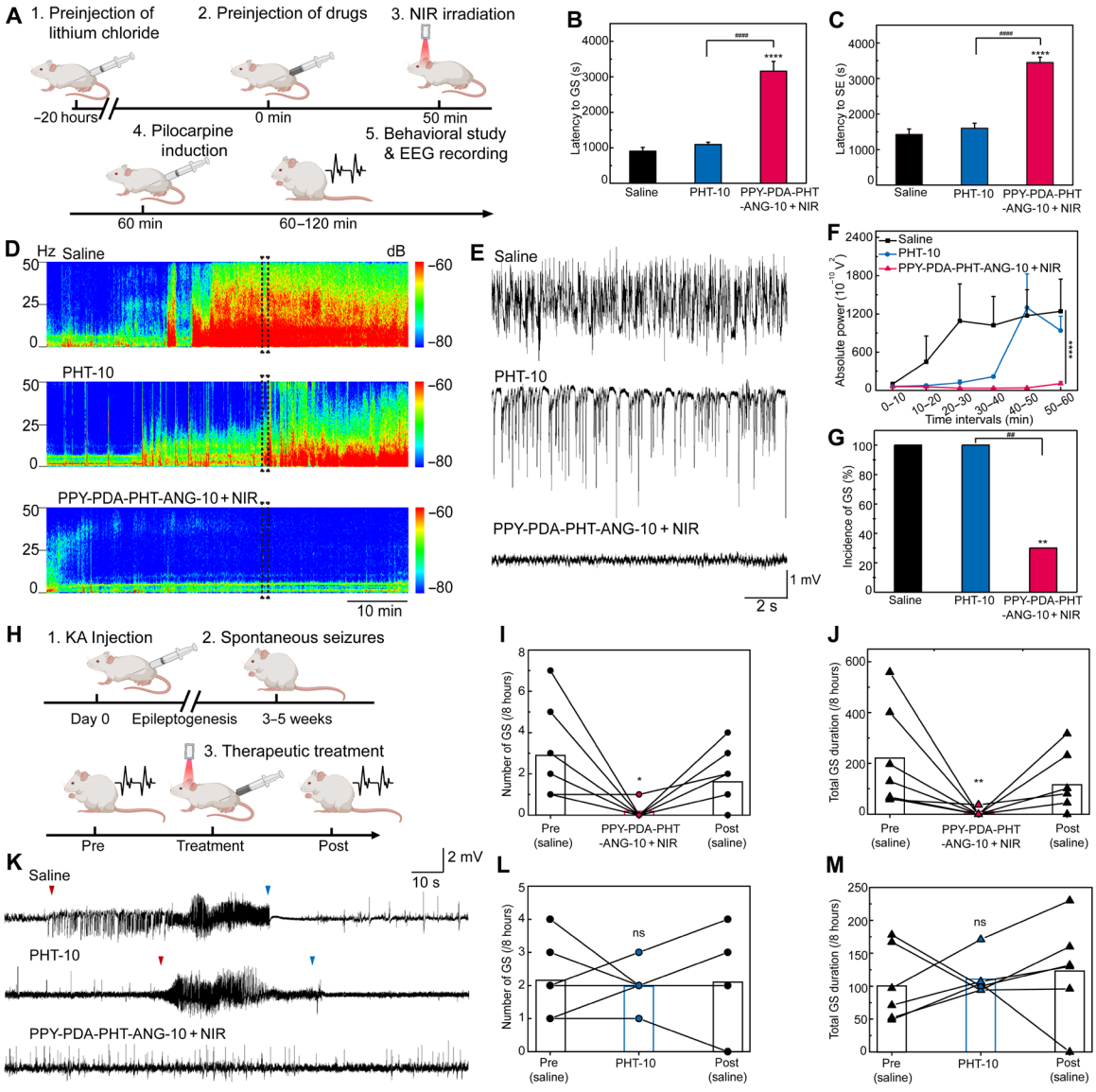

Fig. 4. In vivo antiseizure effects of drug-loaded nanoparticles in pilocarpine-induced SE model and KA-induced chronic epilepsy model. (**A**) Schematic illustration of the control of pilocarpine-induced SE rats via PPY-PDA-PHT-ANG + NIR treatment. (**B**) Latencies to GS and (**C**) to SE of epileptic rats after different treatments of saline, PHT, and PPY-PDA-PHT-ANG + NIR at a dose of 10 mg kg^{-1} ($n = 10$). (**D**) Corresponding power spectral analysis during pilocarpine-induced SE when rats were injected with saline, PHT, and PPY-PDA-PHT-ANG + NIR at a dose of 10 mg kg^{-1}. (**E**) Representative EEGs recorded from the hippocampus of epileptic rats after different treatments at a PHT dose of 10 mg kg^{-1}. (**F**) Power spectral analysis of the EEGs. (**G**) Incidence of GS of pilocarpine-induced SE rats after different treatments ($n = 10$). (**H**) Schematic illustration of the control of KA-induced chronic epileptic rats via PPY-PDA-PHT-ANG + NIR treatment. (**I**) Number and (**J**) duration of GS of the mice treated by PPY-PDA-PHT-ANG-10 + NIR ($n = 7$). (**K**) Representative EEGs recorded from the hippocampus of epileptic rats after different treatments at a PHT dose of 10 mg kg^{-1}. Red and blue triangles indicate the start and the end of one complete GS. (**L**) Number and (**M**) duration of GS of the mice treated by PHT-10 ($n = 6$). ns, not significant.

some inherent defects including unsatisfactory targeting efficiency, potential biotoxicity, and unsustainable drug release mechanism compromised the therapeutic efficacy. In this study, a nanoengineered delivery system was established for on-demand pharmacotherapy of epilepsy. Both in vitro and in vivo studies demonstrated the efficient brain-targeting delivery and superior antiseizure effects with sustained electroresponsive drug release. To the best of our knowledge, the DDS for sustained AED release in response to epileptiform discharges has not been reported previously. Our work thus provides the proof-of-concept study to address the continuous seizure treatment and offers a new perspective of epilepsy pharmacotherapy.

To construct the DDS for AED delivery, pyrrole and dopamine monomers were triggered to copolymerize into sphere nanoparticles and drug molecules were loaded at the meantime. The incorporation of nature-inspired PDA in the DDS showed several advantages. First, the drug loading capacity was improved because of the multiple interactions between PDA and PHT such as hydrogen bonding, electrostatic interactions, and π interactions (*35*). Second, the unique chemistry of PDA makes it feasible for further surface functionalization, enabling the conjugation with PEG polymers and brain-targeting peptides. Third, the hybrid nanoparticles showed distinct light absorbance in the NIR region, suggesting the potential

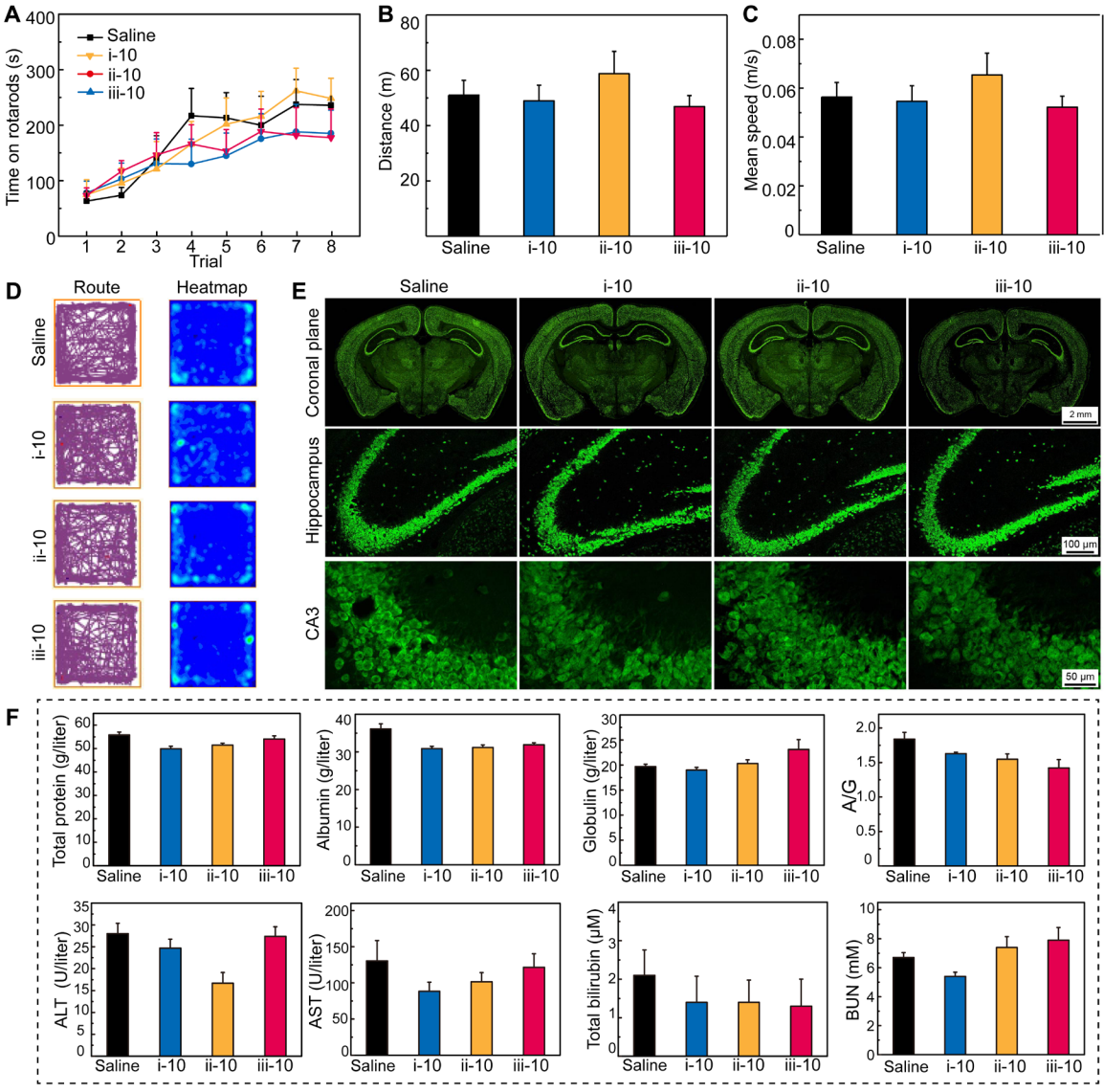

Fig. 5. In vivo biosafety study of the treatment. (**A**) Rotarod analysis of the healthy mice 24 hours after different treatments ($n = 5$). Groups i-10, ii-10, and iii-10 represent the treatment of PHT, PPY-PDA-PHT-ANG, and PPY-PDA-PHT-ANG + NIR at a PHT dose of 10 mg kg^{-1}, respectively. (**B**) Distance and (**C**) mean speed of the mice were recorded over a set time of 15 min under different treatments. (**D**) Typical motion route (left) and heatmap (right) during an open-field test of each different treatment. (**E**) Immunofluorescent images of brain slices from the mice under different treatments. Neurons were stained with NeuN (green). (**F**) Blood chemistry analysis of the mice 7 days after different treatments once a day, including total protein, albumin, globulin, ALT, AST, total bilirubin, and BUN. No obvious difference was found among the four groups.

of photothermal conversion. These motifs contributed to the synergistic brain-targeting strategy, a combination of receptor-mediated transcytosis and BBB disruption–enabled transport, for highly efficient BBB crossing. Moreover, the coassembly of PDA notably improved the drug release sensitivity of the system. It was demonstrated that the AEDs could be released in quick response (as fast as 30 s) to an in vitro electric field. Unlike the electroresponsive hydrogel system, the AEDs encapsulated inside the polymeric system in this work were released upon the reduction by epileptic discharges, leading to a sustained drug release. In vitro releasing profiles under on-off intermittent electric stimuli proved that the PPY-PDA-PHT-ANG system could release the AEDs for at least three times. Note that around 20% of drugs were released in on-off cycles, probably because of the limited stimulation time (3 min in total). Further improvement of the sensitivity was required upon the intermittent discharges. However, current studies have proved that the loaded drugs could be completely released upon continuous stimuli. It is of great importance for effective control of continuous seizures, which has been considered as a bottleneck in traditional AED pharmacotherapy.

To validate the efficacy of electroresponsive drug release for epilepsy, an in vivo acute seizure model was first established. The therapy results demonstrated that PPY-PDA-PHT-ANG with NIR irradiation was able to produce antiseizure effects, confirmed by behavioral studies and EEG recordings. The seizure stage was lowered and the latency to GS was also prolonged, even at a dose of

5 or 10 mg kg^{-1}. Furthermore, we also verified the antiseizure effects in a continuous seizure model, which often fails to be controlled by the delayed AED administration, leading to higher mortality of epilepsy. We found that PHT treatment at a dose of 10 mg kg^{-1} merely has any therapeutic effects on SE mice. However, the key indicators including latency, seizure stage, and EEG severity of the epileptic mice were improved after PPY-PDA-PHT-ANG together with NIR at the same dose. More SE mice survived after the therapy at last, giving lower mortality. These results confirmed that the administration of only one-fifth of the conventional dosage was effective in seizure inhibition. Further KA-induced epileptic model also demonstrated that the PPY-PDA-PHT-ANG nanoparticles were able to inhibit the spontaneous seizure in an established model. The GS number and duration in the recurrent epilepsy model were reduced at a lower dose of PHT. The reduction of regular AED dosage reduces the side effects and decreases the potential evolution of drug-resistant epilepsy, which are the major concerns in epilepsy pharmacotherapy. This improvement could be attributed to the synergistic brain-targeting strategy and sustained drug release triggered by abnormal EEG activities during seizure. For brain targeting, higher distribution of the nanoparticles in the temporal lobe was recorded by ex vivo fluorescence imaging after the combinational treatment. Note that temporal lobe epilepsy is one of the most common types of epilepsy in the clinic (*36*, *37*). In this synergistic targeting strategy, the ANG peptide could target the low-density lipoprotein receptor–related protein 1 and penetrate the BBB through a receptor-mediated transcytosis. In addition, NIR irradiation at the second biowindow modulates the penetration efficiency in a deep and site-specific manner. The NIR-induced BBB opening could quickly return to normal after removing the irradiation, suggesting a precise method for reversible BBB opening. Current studies regarding NIR-related therapy have not been applied on human brain probably because of the limits of NIR device and biosafety concerns. Considering some cases that use NIR regime for brain imaging for nonhuman primates (*38*), we believe that this noninvasive and spatiotemporal method could be used for human brain treatment in the future. For electroresponsive drug release, as revealed by in vivo microdialysis, the initial epileptic discharges in the temporal lobe could trigger the on-demand drug release, thus cutting down the discharge spread in a timely manner. To be specific, the drug concentration in the brain of the PHT group reached its peak at 1 hour and decreased afterward. In comparison, the PPY-PDA-PHT-ANG nanoparticles could respond to seizure onset and epileptic discharges and release more AEDs (350.8%) than the PHT treatment at the same dose. Furthermore, the drug concentration could be maintained at a valid therapeutic level for at least 2 hours. These results proved the on-demand and sustained drug release under electroencephalograph epileptiform abnormalities. Further biosafety study provided a comprehensive evaluation of the biocompatibility and in vivo toxicity of the treatment. The results evidenced that no acute or long-term damages could be found after the administration of PPY-PDA-PHT-ANG together with NIR irradiation, demonstrating the satisfactory biosafety.

In summary, we have developed a nanoengineered DDS and proved its potential use to enhance brain targeting and sustained electroresponsive drug release for on-demand therapy of epilepsy. The surface functionalization by brain-targeting peptide ANG and irradiation-triggered hyperthermia synergistically contributed to an improved drug delivery in the brain. Copolymerized with PDA, the polymeric delivery system showed increased conductivity, sensitivity, and sustained drug release in an electric field. In vivo studies demonstrated its antiepileptic effects in both GS, SE, and spontaneous seizures. Together with the satisfactory results of biosafety evaluation, our work provides a smart strategy for on-demand pharmacotherapy in the fight against epilepsy.

MATERIALS AND METHODS

Chemicals and materials

The pyrrole monomer, ammonium persulfate, and PVA (M_w: ca. 30 kDa) was purchased from Macklin. PHT was purchased from Bidepharm. Dopamine hydrochloride was purchased from Aladdin. ANG (TFFYGGSRGKRNNFKTEEY; 2.3 kDa) was synthesized by the Chinese Peptide Company (Hangzhou, China). The sulfo-Cy5.5 NHS ester and thiol-PEG NHS ester (M_w: 5 kDa) were obtained from Yare Biotech Inc. (Shanghai, China). The Dulbecco's modified Eagle's medium (DMEM), fetal bovine serum (FBS), and 0.25% (w/v) trypsin solution were purchased from Gibco BRL (Gaithersburg, MD, USA). Ultrapure water (18.2 megohms/cm) was purified using a Sartorious AG arium system and used in all experiments. All other chemicals and bioreagents were purchased from Sigma-Aldrich unless otherwise declared.

Characterization

SEM images were obtained on a field-emission scanning electron microscope (SU-8010, Japan). TEM observations were conducted on a JEOL electron microscope (JEM-1400) at an acceleration voltage of 120 kV. UV-Vis-NIR spectra were recorded on a Cary 5000 spectrometer, and fluorescence measurements were recorded on a Horiba spectrofluorometer. The thermogravimetric analysis of the nanoparticles was performed on a Q50 thermogravimetric analyzer. The thermal properties of lyophilized products were then evaluated with a temperature range from room temperature to 800°C (equilibrate at 100°C for 30 min to remove water) under N_2 flow of 40 ml min^{-1}. The hydrodynamic size and surface charge of the nanoparticles were analyzed with a Malvern nanosizer (Nano ZS). Dilute solutions of the as-prepared products (0.2 mg ml^{-1}) were used for the study of hydrodynamic size and zeta potential in neutral buffer (pH 7.2). FTIR spectra were collected on a Nicolet iS50 spectrometer (Thermo Fisher Scientific, USA). Electric resistivity of the nanoparticles (compressed pellet under 20 MPa pressure) was measured by a four-point probe setup (ST2722-SD). NMR spectroscopy was conducted on the AVANCE III 600 MHz Digital NMR Spectrometer. Mass spectra of the polymers were recorded by matrix-assisted laser desorption ionization time of flight (ultrafleXtreme, Bruker). Radiofrequency electromagnetic fields were generated with an Agilent E4421B ESG Series signal generator. Schematic illustrations were created with BioRender.

Synthesis of electroresponsive nanoparticles

The electroresponsive nanoparticles were synthesized in a "one-pot" method. In a typical synthesis, 250 mg of PVA and 10 mg of PHT were dissolved in 10 ml of distilled water by vigorously stirring at room temperature for 1 hour and at 60°C for 30 min. After cooling down to room temperature, 100 μl of 1 M HCl was added to adjust the solution pH. Then, 67 μl of pyrrole and 3.4 mg of dopamine (5% dopamine) was added subsequently under continuous stirring. The polymerization was triggered by adding 100 mg of ammonium

persulfate (predissolved in distilled water). The reaction was allowed for 12 hours under vigorous stirring in the dark. Then, the black products were washed by hot water to remove the unreacted monomers and free PHT molecules for three times and resuspended in distilled water for further use. The drug loading capacity (α) was obtained by Eq. 1

$$\alpha = \frac{(C_0 - C_s)}{C_0} \quad (1)$$

where C_0 and C_s are the original drug concentration and the drug concentration in the supernatant, respectively.

Preparation of ANG-modified nanoparticles

The ANG-modified nanoparticles were synthesized by using NHS-PEG-SH as a linkage between ANG and PDA surface. Briefly, NHS-PEG-SH solution (2 mg ml^{-1}; excessive) was first conjugated to ANG by coupling thiol groups to the amine of the PEG polymer. Unreacted polymer could be removed by dialysis against phosphate-buffered saline (PBS) buffer in the dark. The as-synthesized ANG-PEG-SH was then mixed with PPY-PDA-PHT nanoparticles and was allowed to stir overnight at room temperature. Last, ANG-modified nanoparticles were obtained by centrifugation and washed with PBS buffer for three times to remove unreacted ANG. The purified nanoparticles were stored at 4°C for further use.

In vitro drug release

The in vitro electroresponsive drug release was performed by using two parallel Pt electrodes (1 cm by 1 cm) under electrical stimuli of different current and time in neutral buffer. Before the test, the PPY-PDA-PHT-ANG solution of high nanoparticle concentration (77.5 μl, 4.9 mg ml^{-1}) was first deposited on the Pt surface of cathode and dried under an infrared lamp. The electrodes were then immersed in the buffer (10 ml), and the solution was treated with DC voltage under 50, 100, 200, and 300 μA of current. After a certain time (0.5, 1, 2, 5, or 10 min or 24 hours), of the stimuli, 200 μl of the solution was withdrawn and the PHT concentration was confirmed by HPLC (mobile phase: methanol:water = 65:35).

Computational details

In the present studies, all geometries of reaction species were calculated by means of the M06/6-31G(d,p) method, and frequency calculations were also used to confirm the structures as minimum points in energy and achieve the relevant zero point energy in the gaseous phase. For each transition state, intrinsic reaction coordinate calculations were performed to guarantee its correct connection to the designated local minima. All calculations were implemented via the Gaussian09 software package.

Cell culture and in vitro BBB model

To evaluate the cellular compatibility, the bEnd.3 cell line was cultured in DMEM supplemented with 10% FBS, penicillin (100 IU ml^{-1}), and streptomycin sulfate (100 mg ml^{-1}) [DMEM for bEnd.3 cell culture was additionally supplemented with $NaHCO_3$ (1.5 mg ml^{-1})]. The bEnd.3 cell line was purchased from ZeYe Biological Technology Co. Ltd. (Shanghai, China). The cell lines were cultured in a 5% CO_2 incubator at 37°C. All cellular experiments were performed by using cells in the logarithmic growth phase.

To evaluate the in vitro BBB penetration of ANG-modified nanoparticles, the bEnd.3 cell line was used to build the BBB model according to a reported method (*28*, *29*). Briefly, bEnd.3 cells were seeded in the upper chamber of Transwell plates (6.5-mm Transwell with 0.4-μm Pore Polyester Membrane Insert; Corning) at a density of 3×10^4 cells per well to form a tight monolayer. The culture medium was changed every other day, and the TEER was measured everyday using an EVOM^2 instrument (World Precision Instruments Inc., USA) and STX2 electrode. When the TEER reached 200 ohm·cm^{-2}, the medium in the upper chamber was replaced with PPY-PDA-PHT-ANG solutions dispersed in Hepes-KRH buffer [136 mM NaCl, 0.9 mM $CaCl_2$, 0.5 mM $MgCl_2$, 2.7 mM KCl, 1.5 mM KH_2PO_4, 10 mM NaH_2PO_4, 25 mM glucose, and 10 mM Hepes (pH 7.4)]. Afterward, the cell monolayer was irradiated with NIR laser for 10 min (300 mW cm^{-2}). The drug concentration in the down chamber was measured using HPLC. The penetration efficiency (β) across the in vitro BBB model was determined by Eq. 2

$$\beta = \frac{(Ct - Cd)}{Ct} \quad (2)$$

where *Ct* and *Cd* are the total drug concentration and the drug concentration in the down chamber, respectively.

Photothermal conversion study

Photothermal conversion tests were carried on using 400 μl of PPY-PDA-PHT-ANG at different concentrations under NIR irradiation (1064 nm) in 1.5-ml tubes, and the temperature change was recorded with an infrared camera every 30 s. To obtain the photothermal conversion efficiency (η), PPY-PDA-PHT-ANG solution [optical density at 1064 nm (OD_{1064}) = 1] suspended in a quartz cuvette was exposed to a NIR laser for 20 min and the temperature was recorded in the heating and natural cooling stage. The efficiency η was calculated according to Eq. 3 reported before as follows

$$\eta = \frac{hS(T_{max} - T_{surr}) - hS(T_{max.water} - T_{surr})}{P(1 - 10^{-A1064})} \quad (3)$$

where *h* is the heat transfer coefficient; *S* is the surface area of sample container; T_{max}, T_{surr}, and $T_{max.water}$ are the highest temperature the sample reached, the ambient room temperature, and the highest temperature the water reached, respectively; *P* is the laser power density; and A_{1064} is the localized surface plasmon resonance absorbance of PPY-PDA-PHT-ANG solution at 1064 nm. The value of *hS* in the equation above is calculated by Eq. 4

$$hS = \frac{mc + m'c'}{\tau} \quad (4)$$

where *m*, *m*′, *c*, and *c*′ are the mass of PPY-PDA-PHT-ANG solution and the quartz cuvette as well as the heat capacity of the solution and the quartz cuvette, respectively. The value of τ is the characteristic thermal time constant that can be determined from the curve of sample cooling time versus negative natural logarithm of the temperature driving force $\left(\frac{\Delta T}{\Delta T_{max}}\right)$.

Animals

Male mice (6 to 8 weeks; ICR and C57BL/6J) and male rats [6 to 8 weeks; Sprague-Dawley (SD)] with normal immune status were maintained in individual cages with a 12-hour light-dark cycle (lights on from 08:00 to 20:00) supplemented with sterile food and

water, and they were not treated by any other behavior tests or drugs before. After the therapy, animals were separately housed. All behavior tests were conducted between 09:00 and 18:00. All animal experiments were performed in compliance with the Laboratory Animal Welfare and Ethics Committee of Zhejiang University and the National Institutes of Health *Guide for the Care and Use of Laboratory Animals*.

Ex vivo fluorescence imaging

To study the BBB penetration of ANG-modified nanoparticles, the NIR fluorescent dye Cy5.5 was used as a fluorescent marker for ex vivo brain imaging. Before use, PPY-PDA-PHT and PPY-PDA-PHT-ANG nanoparticles were both conjugated with NHS–ester Cy5.5, and excessive dye molecules were removed by centrifugation. Then, male ICR mice were randomly divided into four groups (n = 3) with different treatment: (i) control (PPY-PDA-PHT only), (ii) NIR (PPY-PDA-PHT with NIR irradiation), (iii) ANG (PPY-PDA-PHT-ANG), and (iv) NIR + ANG (PPY-PDA-PHT-ANG with NIR irradiation). After 50 min of injection of dye-labeled nanoparticles (PHT concentration: 10 mg kg^{-1} of body weight) at the same concentration, the mouse brains of groups ii and iv were irradiated by NIR irradiation for 10 min, focusing on the temporal lobe area. The surface temperature of the brain skin was monitored and kept below 43°C with a thermal infrared camera to avoid hyperthermal damage. Then, mice in all groups were perfused with saline and the corresponding brains were prepared. The fluorescence imaging was conducted using an IVIS Spectrum animal imager. For Allen Brain Atlas, CPu = caudate putamen (striatum), NAc = nucleus accumbens, dHip = dorsal hippocampus, MD = mediodorsal thalamic nucleus, vHip = ventral hippocampus, SN = substantia nigra, and VTA = ventral tegmental area.

PTZ-induced seizure model for epilepsy therapy

ICR mice were randomly divided into seven groups (n = 10) with different intraperitoneally injected drugs. (i-5) PHT solution (5 mg kg^{-1}), (i-10) PHT solution (10 mg kg^{-1}), (ii-5) PPY-PDA-PHT solution (5 mg kg^{-1}), (ii-10) PPY-PDA-PHT solution (10 mg kg^{-1}), (iii-5) PPY-PDA-PHT-ANG + NIR (5 mg kg^{-1}), and (iii-10) PPY-PDA-PHT-ANG + NIR (10 mg kg^{-1}). After 50 min of injection, groups iii-5 and iii-10 were irradiated by NIR irradiation (1064 nm) for 10 min, focusing on the temporal lobe area. After 60 min of the injection, all groups were intraperitoneally injected with PTZ (100 mg kg^{-1}). Mice were then evaluated for seizure severity and EEG monitoring (PowerLab, AD Instruments) in the next 30 min according to our previous report (*39*). Seizure severity was scored in according with Racine scale: 1, immobilization and facial movement; 2, head nodding; 3, unilateral forelimb clonus; 4, bilateral forelimb clonus with rearing; 5, jumping and falling; and 6, tonic-clonic convulsions and hindlimb extension.

For EEG monitoring, mice were anesthetized with intraperitoneal injection of sodium pentobarbital (60 mg kg^{-1}) and immobilized in a stereotaxic apparatus. Two metallic screws were placed over the sensorimotor cortex as the recording electrodes and another over the cerebellum as the reference. All screws were then secured by dental cement. After the surgery, mice were allowed for 5 to 7 days of recovery before PTZ induction.

Microdialysis

The microdialysis was performed according to our previous report (*39*). Briefly, ICR mice were first randomly divided into three groups (n = 3). Then, mice were chronically implanted with guide cannulae (CMA/12 polyurethane; Carnegie Medicine, Stockholm, Sweden) into the right ventral hippocampus under sodium pentobarbital anesthesia (60 mg kg^{-1}, intraperitoneally). The cannula was held in place with three screws that were attached to the skull with dental cement. After 5 to 7 days of recovery, microdialysis probes (CMA/12, molecular weight cutoff of 20 kDa; Carnegie Medicine) were lowered through the guide cannula, and the mice were placed in a freely moving system, consisting of a plastic cylinder with a counterbalancing arm carrying a two-channel swivel (Carnegie Medicine). After balancing for 1 hour after insertion, the perfusion was conducted by using artificial cerebrospinal fluid (125 mM NaCl, 2.5 mM KCl, 1.18 mM $MgCl_2$, and 1.26 mM $CaCl_2$). The inflow to the probe was driven with a CMA/100 microinjection pump (flow rate: 2.0 μl min^{-1}), and a 60-μl outflow sample was collected every 30 min. After drug administration of PHT, PPY-PDA-PHT-ANG-10, or PPY-PDA-PHT-ANG-10 + NIR, eight samples were collected over the next 4 hours. The PHT concentration was determined by HPLC with a UV detector. Before each microdialysis probe used for in vivo test, in vitro recovery was determined to calculate the corrected dialysate concentration by dialysis of a stirred artificial cerebrospinal fluid solution containing PHT (5 μg ml^{-1}).

Pilocarpine-induced SE model for epilepsy therapy

SD rats were pretreated with lithium chloride (3 meq kg^{-1}, intraperitoneally) 20 hours before and then randomly divided into four groups (n = 10). The rats were then injected (intraperitoneally) with (i) saline, (ii) PHT solution (10 mg kg^{-1}), and (iii) PPY-PDA-PHT-ANG (10 mg kg^{-1}) with NIR irradiation. After 50 min of injection, rats of group iv were irradiated by NIR irradiation (1064 nm) for 10 min, focusing on the temporal lobe area. After 60 min of the injection, all groups were intraperitoneally injected with pilocarpine (30 mg kg^{-1}) and were evaluated for seizure severity in the next 60 min. Seizure severity was scored in accordance with Racine scale as mentioned above.

KA-induced chronic epilepsy model for epilepsy therapy

For KA injection, C57BL/6J (wild type) mice were anesthetized with ~2% isoflurane and mounted in a stereotaxic apparatus; KA (0.5 mg/ml, 0.5 μl; ab120100, Abcam) was injected into the dorsal hippocampus (antero-posterior, −2.0 mm; lateral, −1.2 mm; ventral, −1.6 mm) with a glass pipette attached to a syringe at 100 nl min^{-1}. After each injection, the pipette was left in place for 5 min before withdrawal. Then, twisted bifilar stainless electrodes were implanted into the hippocampal CA3 (antero-posterior, −2.9 mm; lateral, −3.1 mm; ventral, −3.1 mm) for EEG recording.

Three to 5 weeks after KA injection and recovery, EEG was monitored (PowerLab, AD Instruments) in freely moving mice, which was synchronized with video recording continuously for 8 hour/day. In the first day (pretreatment), each mouse was intraperitoneally injected with saline before the recording start. GS was defined as a paroxysmal event that continued over 30 s, accompanied by a marked tonic-clonic behavior. FS was defined as a paroxysmal event that continued more than 10 s and had an average amplitude of three times versus baseline and frequency of >2 Hz (*40*). Only mice with detectable seizures were given subsequent treatment. In the second day (treatment), each mouse was intraperitoneally injected with PHT (10 mg kg^{-1}) or PPY-PDA-PHT-ANG (10 mg kg^{-1}) with NIR before the recording start. Mice were then injected with saline on posttreatment day.

Open-field test

ICR mice were randomly divided into four groups (n = 5) with different intraperitoneally injected drugs: (i) vehicle control, (ii) PHT solution (10 mg kg^{-1}), (iii) PPY-PDA-PHT (10 mg kg^{-1}), and (iv) PPY-PDA-PHT-ANG (10 mg kg^{-1}) with NIR irradiation. The test was performed after 24 hours of the injection. Before the test, all mice were habituated in the test room for at least 1 hour to acclimatize the environment. Three boxes (45 cm by 45 cm by 45 cm) with an open top and black underside were used at a time. The open field was set for 15 min from the time of mouse insertion into the box. The boxes should be cleaned before and after every test. The motion trail of each mouse was captured, and the total distance and average speed were recorded.

Rotarod test

The rotarod test was performed to measure the motor coordination of the rodents according to our previous report (*39*). ICR mice were randomly divided into four groups (n = 5) with different intraperitoneally injected drugs: (i) vehicle control, (ii) PHT solution (10 mg kg^{-1}), (iii) PPY-PDA-PHT (10 mg kg^{-1}), and (iv) PPY-PDA-PHT-ANG (10 mg kg^{-1}) with NIR irradiation. The test was performed after 24 hours of the injection. Before the test, all mice were placed in the test room for at least 1 hour to acclimatize the environment and stayed on the rotarod apparatus (YLS-4C) for 2 min to maintain balance. Then, the cylinder was rotating from 0 to 40 rpm in 2 min as one trial went on, and then rotated with a fixed speed for another 3 min. Each mouse received eight trials with 20-min interval, except that the fourth and fifth rounds are 1 hour apart. The latency that mice remained on the rod in each trial was recorded.

Blood chemistry

ICR mice were treated different treatments: (i) vehicle control, (ii) PHT solution (10 mg kg^{-1}), (iii) PPY-PDA-PHT (10 mg kg^{-1}), and (iv) PPY-PDA-PHT-ANG (10 mg kg^{-1}) with NIR irradiation once a day for 1 week. After the treatment, the mice were anesthetized by isoflurane and the blood samples were collected from the eyes. After cooling down at 4°C overnight, the samples were centrifuged (4000 rpm, 10 min) and the supernatants were collected for hemobiocompatibility analysis. The hematological parameters including total protein, albumin, globulin, total bilirubin, ALT, AST, and BUN were measured for each sample. (n = 5).

Immunohistochemistry

After the treatment, ICR mice were deeply anesthetized with intraperitoneal injection of sodium pentobarbital (100 mg kg^{-1}) and transcardially perfused with 4% (w/v) paraformaldehyde (PFA). The major organs (heart, liver, spleen, lung, and kidney) and brains were harvested for further study. For hematoxylin and eosin (H&E) staining, paraffin-embedded sectioning was performed and the staining was finished according to the standard protocol. The organs and brains were fixed in 4% PFA and dehydrated with sucrose solution (mass concentration of 15 and 30%) for 24 hours. The samples were then sliced into frozen sections with 2-μm thickness, and H&E staining was finished. For NeuN staining, brains were first fixed in 4% PFA at 4°C overnight and then cryoprotected completely with 30% sucrose. Twenty-micrometer coronal slices were cut on a freezing microtome (Thermo Fisher Scientific). Slices were processed for immunofluorescence for primary antibody rabbit anti-NeuN (1:500; MABN140, Millipore), rabbit anti-GFAP (glial fibrillary acidic protein) (1:500; BA0056, BOSTER), and goat anti-Iba1 (1:500; ab5076, Abcam); diluted in 1% PBS at 4°C overnight; rinsed with 1% PBS next; and then incubated with an Alexa Fluor 488–conjugated secondary fluorescent antibody (1:500; Jackson ImmunoResearch) at room temperature for 2 hours. Slices were finally mounted and assessed the immunofluorescence with a confocal microscope (Leica).

Statistical analysis

The data are presented as means ± SEM, and a two-tailed P value of <0.05 was considered statistically significant in all cases. A one-way ANOVA with Dunnett's multiple comparisons test was used to compare the seizure stages, latencies, and microdialysis results. A one-way ANOVA with Dunn's multiple comparisons test was used to compare the number and duration of GS and FS in a spontaneous model. A two-way ANOVA with Tukey's multiple comparisons test was used to compare the absolute power of EEGs. The chi-square test was used to compare the survival rate and incidence of GS and SE.

SUPPLEMENTARY MATERIALS

Supplementary material for this article is available at https://science.org/doi/10.1126/sciadv.abm3381

View/request a protocol for this paper from *Bio-protocol*.

REFERENCES AND NOTES

1. O. Devinsky, A. Vezzani, T. J. O'Brien, N. Jette, I. E. Scheffer, M. de Curtis, P. Perucca, Epilepsy. *Nat. Rev. Dis. Primers* **4**, 18024 (2018).
2. J. O. McNamara, Cellular and molecular basis of epilepsy. *J. Neurosci.* **14**, 3413–3425 (1994).
3. W. Löscher, H. Klitgaard, R. E. Twyman, D. Schmidt, New avenues for anti-epileptic drug discovery and development. *Nat. Rev. Drug Discov.* **12**, 757–776 (2013).
4. H. Potschka, W. Löscher, In vivo evidence for P-glycoprotein–mediated transport of phenytoin at the blood–brain barrier of rats. *Epilepsia* **42**, 1231–1240 (2001).
5. J. A. Cramer, S. Mintzer, J. Wheless, R. H. Mattson, Adverse effects of antiepileptic drugs: A brief overview of important issues. *Expert. Rev. Neurother.* **10**, 885–891 (2010).
6. V. R. Yasam, V. Senthil, S. L. Jakki, N. Jawahar, Status epilepticus: An overview. *Curr. Drug Metab.* **18**, 174–185 (2017).
7. X. Guo, G. Deng, J. Liu, P. Zou, F. Du, F. Liu, A. T. Chen, R. Hu, M. Li, S. Zhang, Z. Tang, L. Han, J. Liu, K. N. Sheth, Q. Chen, X. Gou, J. Zhou, Thrombin-responsive, brain-targeting nanoparticles for improved stroke therapy. *ACS Nano* **12**, 8723–8732 (2018).
8. S. Ruan, Y. Zhou, X. Jiang, H. Gao, Rethinking CRITID procedure of brain targeting drug delivery: Circulation, blood brain barrier recognition, intracellular transport, diseased cell targeting, internalization, and drug release. *Adv. Sci.* **8**, 2004025 (2021).
9. M. Agrawal, S. Saraf, S. Saraf, S. K. Dubey, A. Puri, U. Gupta, P. Kesharwani, V. Ravichandiran, P. Kumar, V. G. M. Naidu, U. S. Murty, Ajazuddin, A. Alexander, Stimuli-responsive In situ gelling system for nose-to-brain drug delivery. *J. Control. Release* **327**, 235–265 (2020).
10. X. Ying, Y. Wang, J. Liang, J. Yue, C. Xu, L. Lu, Z. Xu, J. Gao, Y. Du, Z. Chen, Angiopep-conjugated electro-responsive hydrogel nanoparticles: Therapeutic potential for epilepsy. *Angew. Chem. Int. Ed.* **53**, 12436–12440 (2014).
11. J. Liu, Y. He, J. Zhang, J. Li, X. Yu, Z. Cao, F. Meng, Y. Zhao, X. Wu, T. Shen, Z. Hong, Functionalized nanocarrier combined seizure-specific vector with P-glycoprotein modulation property for antiepileptic drug delivery. *Biomaterials* **74**, 64–76 (2016).
12. Z. Fang, S. Chen, J. Qin, B. Chen, G. Ni, Z. Chen, J. Zhou, Z. Li, Y. Ning, C. Wu, L. Zhou, Pluronic P85-coated poly(butylcyanoacrylate) nanoparticles overcome phenytoin resistance in P-glycoprotein overexpressing rats with lithium-pilocarpine-induced chronic temporal lobe epilepsy. *Biomaterials* **97**, 110–121 (2016).
13. J. Zhao, Z. Ye, J. Yang, Q. Zhang, W. Shan, X. Wang, Z. Wang, S. Ye, X. Zhou, Z. Shao, L. Ren, Nanocage encapsulation improves antiepileptic efficiency of phenytoin. *Biomaterials* **240**, 119849 (2020).
14. W. Tang, W. Fan, J. Lau, L. Deng, Z. Shen, X. Chen, Emerging blood–brain-barrier-crossing nanotechnology for brain cancer theranostics. *Chem. Soc. Rev.* **48**, 2967–3014 (2019).
15. Y. Jiang, W. Yang, J. Zhang, F. Meng, Z. Zhong, Protein toxin chaperoned by LRP-1-targeted virus-mimicking vesicles induces high-efficiency glioblastoma therapy in vivo. *Adv. Mater.* **30**, e1800316 (2018).
16. M. Choi, T. Ku, K. Chong, J. Yoon, C. Choi, Minimally invasive molecular delivery into the brain using optical modulation of vascular permeability. *Proc. Natl. Acad. Sci. U.S.A.* **108**, 9256–9261 (2011).

17. W. Chen, J. Ouyang, X. Yi, Y. Xu, C. Niu, W. Zhang, L. Wang, J. Sheng, L. Deng, Y. Liu, S. Guo, Black phosphorus nanosheets as a neuroprotective nanomedicine for neurodegenerative disorder therapy. *Adv. Mater.* **30**, 1703458 (2018).
18. L. Jin, P. Hu, Y. Wang, L. Wu, K. Qin, H. Cheng, S. Wang, B. Pan, H. Xin, W. Zhang, X. Wang, Fast-acting black-phosphorus-assisted depression therapy with low toxicity. *Adv. Mater.* **32**, 1906050 (2020).
19. G. Hong, A. L. Antaris, H. Dai, Near-infrared fluorophores for biomedical imaging. *Nat. Biomed. Eng.* **1**, 0010 (2017).
20. J. Li, H. Duan, K. Pu, Nanotransducers for near-infrared photoregulation in biomedicine. *Adv. Mater.* **31**, 1901607 (2019).
21. C. Xu, K. Pu, Second near-infrared photothermal materials for combinational nanotheranostics. *Chem. Soc. Rev.* **50**, 1111–1137 (2021).
22. Y. Cai, Z. Wei, C. Song, C. Tang, W. Han, X. Dong, Optical nano-agents in the second near-infrared window for biomedical applications. *Chem. Soc. Rev.* **48**, 22–37 (2019).
23. P. Yang, F. Zhu, Z. Zhang, Y. Cheng, Z. Wang, Y. Li, Stimuli-responsive polydopamine-based smart materials. *Chem. Soc. Rev.* **50**, 8319–8343 (2021).
24. W. Cheng, X. Zeng, H. Chen, Z. Li, W. Zeng, L. Mei, Y. Zhao, Versatile polydopamine platforms: Synthesis and promising applications for surface modification and advanced nanomedicine. *ACS Nano* **13**, 8537–8565 (2019).
25. E. Chalmers, H. Lee, C. Zhu, X. Liu, Increasing the conductivity and adhesion of polypyrrole hydrogels with electropolymerized polydopamine. *Chem. Mater.* **32**, 234–244 (2020).
26. W. Zhang, Z. Pan, F. K. Yang, B. Zhao, A facile in situ approach to polypyrrole functionalization through bioinspired catechols. *Adv. Funct. Mater.* **25**, 1588–1597 (2015).
27. C. Wang, W. Sun, J. Zhang, J. Zhang, Q. Guo, X. Zhou, D. Fan, H. Liu, M. Qi, X. Gao, H. Xu, Z. Gao, M. Tian, H. Zhang, J. Wang, Z. Wei, N. J. Long, Y. Mao, C. Li, An electric-field-responsive paramagnetic contrast agent enhances the visualization of epileptic foci in mouse models of drug-resistant epilepsy. *Nat. Biomed. Eng.* **5**, 278–289 (2021).
28. H. He, Y. Li, X. Jia, J. Du, X. Ying, W. Lu, J. Lou, Y. Wei, PEGylated poly(amidoamine) dendrimer-based dual-targeting carrier for treating brain tumors. *Biomaterials* **32**, 478–487 (2011).
29. X. Jiang, H. Xin, Q. Ren, J. Gu, L. Zhu, F. Du, C. Feng, Y. Xie, X. Sha, X. Fang, Nanoparticles of 2-deoxy-d-glucose functionalized poly(ethylene glycol)-co-poly(trimethylene carbonate) for dual-targeted drug delivery in glioma treatment. *Biomaterials* **35**, 518–529 (2014).
30. A. Lüttjohann, P. F. Fabene, G. van Luijtelaar, A revised Racine's scale for PTZ-induced seizures in rats. *Physiol. Behav.* **98**, 579–586 (2009).
31. C. Xu, Y. Wang, S. Zhang, J. Nao, Y. Liu, Y. Wang, F. Ding, K. Zhong, L. Chen, X. Ying, S. Wang, Y. Zhou, S. Duan, Z. Chen, Subicular pyramidal neurons gate drug resistance in temporal lobe epilepsy. *Ann. Neurol.* **86**, 626–640 (2019).
32. P. Perucca, F. G. Gilliam, Adverse effects of antiepileptic drugs. *Lancet Neurol.* **11**, 792–802 (2012).
33. S. Naqvi, A. Panghal, S. Flora, Nanotechnology: A promising approach for delivery of neuroprotective drugs. *Front. Neurosci.* **14**, 494 (2020).
34. M. Shringarpure, S. Gharat, M. Momin, A. Omri, Management of epileptic disorders using nanotechnology-based strategies for nose-to-brain drug delivery. *Expert Opin. Drug Del.* **18**, 169–185 (2021).
35. D. Wu, J. Zhou, M. N. Creyer, W. Yim, Z. Chen, P. B. Messersmith, J. V. Jokerst, Phenolic-enabled nanotechnology: Versatile particle engineering for biomedicine. *Chem. Soc. Rev.* **50**, 4432–4483 (2021).
36. E. Krook-Magnuson, C. Armstrong, M. Oijala, I. Soltesz, On-demand optogenetic control of spontaneous seizures in temporal lobe epilepsy. *Nat. Commun.* **4**, 1376 (2013).
37. B. Bell, J. J. Lin, M. Seidenberg, B. Hermann, The neurobiology of cognitive disorders in temporal lobe epilepsy. *Nat. Rev. Neurol.* **7**, 154–164 (2011).
38. Z. Sheng, Y. Li, D. Hu, T. Min, D. Gao, J.-S. Ni, P. Zhang, Y. Wang, X. Liu, K. Li, H. Zheng, B. Z. Tang, Centimeter-deep NIR-II fluorescence imaging with nontoxic AIE probes in nonhuman primates. *Research* **2020**, 4074593 (2020).
39. Y. Wang, X. Ying, L. Chen, Y. Liu, Y. Wang, J. Liang, C. Xu, Y. Guo, S. Wang, W. Hu, Y. Du, Z. Chen, Electroresponsive nanoparticles improve antiseizure effect of phenytoin in generalized tonic-clonic seizures. *Neurotherapeutics* **13**, 603–613 (2016).
40. B. Chen, C. Xu, Y. Wang, W. Lin, Y. Wang, L. Chen, H. Cheng, L. Xu, T. Hu, J. Zhao, P. Dong, Y. Guo, S. Zhang, S. Wang, Y. Zhou, W. Hu, S. Duan, Z. Chen, A disinhibitory nigra-parafascicular pathway amplifies seizure in temporal lobe epilepsy. *Nat. Commun.* **11**, 923 (2020).

Acknowledgments

Funding: This project was supported by grants from the National Natural Science Foundation of China (82003666, 81630098, 82022071, and 81821091) and China Postdoctoral Science Foundation (2020M671773 and 2020TQ0266). **Author contributions:** D.W., Y.W., and Z.C. conceived and designed the project. D.W., F.F., Q.Z., X.W., Y.G., and X.C. performed the experimental work. D.W., F.F., Q.Z., Y.Z., B.T., C.X., H.X., W.F., and Y.W. analyzed the data. D.W., F.F., Y.W., and Z.C. wrote the manuscript. All authors discussed the results and contributed to the final manuscript. **Competing interests:** D.W., F.F., Y.W., and Z.C. are inventors on a patent application related to this work filed by Zhejiang University (no. 202011402892.X, filed on 02 December 2020). The authors declare that they have no other competing interests. **Data and materials availability:** All data needed to evaluate the conclusions in the paper are present in the paper and/or the Supplementary Materials. Additional data related to this paper may be also obtained from https://doi.org/10.6084/m9.figshare.17139989.

Submitted 10 September 2021
Accepted 19 November 2021
Published 12 January 2022
10.1126/sciadv.abm3381